JOURNAL OF MATERIALS SCIENCE 27 (1992) 29–35

Structure, nucleation, growth and morphology of secondary carbides in high chromium and Cr–Ni white cast irons

G. L. F. POWELL
CSIRO Division of Manufacturing Technology, P.O. Box 4, Woodville, South Australia 5051
G. LAIRD II
Albany Research Centre, US Bureau of Mines, P.O. Box 70, Albany, OR 97321, USA

Heat-treated high chromium and Cr–Ni white cast irons are widely used by the mining and mineral industries for impact and abrasion resistance. With certain heat treatments, Fe–Cr carbides are precipitated within the chromium- and carbon-rich austenitic matrix, thereby destabilizing the austenite which transforms substantially to martensite on subsequent cooling. The crystal structures of these carbides were determined indirectly by referring electron microprobe analyses of the austenitic matrix to the appropriate isothermal solid-state sections of the Fe–Cr–C phase diagram and directly by microprobe analyses of exposed secondary carbides. The nucleation, growth and morphology of these carbides were studied by a combination of selective removal of the austenitic matrix and subsequent scanning electron microscopy of the exposed carbides.

1. Introduction

The microstructure of highly alloyed hypoeutectic chromium and Cr–Ni white cast irons can be described as an anomalous eutectic [1]. The matrix of austenite (γ-Fe) in these alloys surrounds an interconnecting network of brittle faceted $(Cr, Fe)_7C_3$ or $(Fe, Cr)_7C_3$ (M_7C_3) eutectic carbides [2–4].

These materials are dominantly used in the mining and mineral processing industries for wear resistance [5–7]. To obtain improved repetitive-impact toughness and (depending upon the wear environment) improved abrasion resistance, these irons are often heat treated at temperatures above the A3 temperature, held, and then furnace cooled [8, 9]. The purpose of this heat treatment is to transform the softer metastable austenitic matrix to a harder and more stable martensitic matrix [7, 9].

An often ignored side-product of the heat treatment is the formation of numerous Fe–Cr carbides formed by the solid-state reaction of γ-Fe $\rightarrow M_3C$ or M_7C_3 or $M_{23}C_6 + \gamma$-Fe. Carbides formed via this solid-state reaction are often termed secondary carbides. The formation of these carbides and the attendant dealloying of chromium and carbon of the matrix is essential to the transformation of austenite to martensite upon cooling [7]. Furthermore, it has been shown by others that secondary carbides play an important role in determining the toughness and abrasion resistance of high-alloy white cast irons [7]. Therefore, these irons should be viewed as having three major components that influence their wear properties; a matrix of martensite and some austenite, M_7C_3 eutectic carbides, and secondary carbides.

The structure, nucleation, growth, and morphology of secondary carbides in a range of hypoeutectic chromium and Cr–Ni white cast irons were investigated. The structures of various secondary carbides were inferred from electron microprobe measurements of chromium and carbon in the austenite dendrites with reference to the Fe–Cr–C phase diagram and electron microprobe analyses of exposed individual carbides. Nucleation and growth mechanisms were postulated from scanning electron microscopy (SEM) observations. Lastly, the morphology of these carbides is shown by SEM observations.

2. Experimental procedure

All specimens used for this study were melted in induction furnaces and cast into chemically bonded sand moulds. Table I gives their compositions and cooling rates during solidification in the sand mould. Compositions were determined by X-ray fluorescence on 25.4 mm round bars for the heavy elements and gaseous diffusion for carbon. The cooling rate was calculated as the elapsed time between the eutectic

TABLE I Irons studied

Alloy	Composition (wt %)						Cooling rate (K s^{-1})
	Cr	Ni	C	Si	Mn	Mo	
A	8.8	5.7	3.0	1.8	1.1	0.0	0.15
B	17.7	0.4	3.1	0.2	0.6	1.1	0.15
C	29.3	0.1	2.5	0.1	0.1	0.0	0.30

0022–2461/92 $03.00 + .12

TABLE II Heat-treatment details

Alloy	Temperature (K)	Soak (h)
A1	As-cast	None
A2	1073	0.25
A3	1073	0.75
A4	1073	4.00
B1	As-cast	None
B2	1273	0.25
B3	1273	0.75
B4	1273	4.00
C1	As-cast	None
C2	1273	0.25
C3	1273	0.75
C4	1273	4.00

arrest temperature and 873 K. These temperatures were measured by an alumina-sheathed Type S thermocouple inserted into the casting cavity.

Alloys A and C were melted from starting materials of pig iron, electrolytic nickel and chromium and ferrous-based compounds of silicon and manganese. Alloy B was obtained from a commercial foundry. Specimens were cut from each alloy using a slow-speed water-cooled tungstencarbide bandsaw. To prevent decarburization, the specimens were wrapped in several layers of stainless steel foil before heat treating. A pre-heated furnace was used in all heat treatments and after the prescribed isothermal soak, the specimens were air cooled. Table II gives the heat treatments and hold times.

The use of 1073 K (Alloy A) and 1273 K (Alloys B and C) isothermal soak temperatures and times up to 4 h follow commercial practice for austenite destabilization for these irons [10, 11]. The lower temperature of 1073 K results from the addition of nickel to Alloy A. The increased nickel content depresses the solid state reaction of $\gamma\text{-Fe} \rightarrow \gamma\text{-Fe} + \alpha\text{-Fe}$ + carbide to a lower temperature [12]. Hence, for all alloys, the solid-state reaction at these temperatures is one of $\gamma\text{-Fe} \rightarrow \text{carbide} + \gamma\text{-Fe}$ [13, 14]. Subsequent to casting and heat treating, the specimens were mounted in epoxy and polished using standard metallographic techniques.

2.2. Analytical procedures used

To reveal the secondary carbides in the above specimens, the austenitic matrix was chemically dissolved in a solution of 75% concentrated HCl, 24% concentrated HNO_3, and 1% concentrated HF. The deep-etched microstructures were then observed via the secondary electron imaging mode in a scanning electron microscope.

The compositions of the carbides and matrix phases reported in this paper were determined with a Cameca SX-50 electron microprobe fitted with wavelength-dispersive spectrometers. Each spectrometer was peaked for a particular element (Mo, Fe, Cr, Ni, Mn, Si, and C), and its output was calibrated against known standards. The most critical of the standards, that for carbon, was the primary M_7C_3 carbide present in a high-chromium white cast iron. $K_{\alpha 1}$ radiation was always used. Count times were 50 s for carbon and 10 s for all other elements. The beam current and accelerating voltage were held constant at 0.020 μA and 15 kV, respectively. Under these operating conditions, fluorescence occurred in a region with a linear dimension of ~ 2 μm and a volume of 6–8 μm^3. The beam could be positioned on the surface of the specimen with an accuracy of ± 1 μm.

3. Results and discussion

3.1. Structure

To determine the composition of the eutectic carbides and the microsegregation of alloying elements within the austenite dendrites, microprobe traverses were performed across dendrites in Alloys A1, B1 and C1. Selected analyses and summary statistics from this work are given in Table III. The final column of Table III labelled "Stoichiometry", gives the metal (M = Fe + Cr + Ni + Mn + Mo) to carbon ratio for each analysis of a carbide. Thereby, because the carbide types M_3C, M_7C_3, and $M_{23}C_6$ have been found to be almost completely stoichiometric [4, 13, 15–17], the analyses given in Table III show that all three alloys have eutectic carbides of the M_7C_3 type. Work by Laird *et al.* [4] (approximating to Alloy A) and Jackson [14] and Thorpe and Chicco [18] (approximating to Alloys B and C) has shown that these

TABLE III Microprobe analyses across eutectic carbides and austenite dendrites (composition in wt %)

Alloy	Fe	Cr	Ni	C	Si	Mn	Mo	Total	Mean	COV[a]	Stoichiometry
A1											
γ-Fe[b]	84.1	4.7	7.3	1.4	2.0	0.8	0.0	100.3	100.3	0.4	n/a
EC[c]	58.4	31.8	0.8	8.6	0.0	1.2	0.0	100.8			$M_{70}C_{30}$
B1											
γ-Fe	85.8	10.1	0.5	1.2	0.4	0.5	0.4	98.9	99.2	0.6	n/a
EC	46.3	43.8	0.0	8.6	0.0	0.5	1.9	101.3			$M_{70}C_{30}$
C1											
γ-Fe	79.8	19.3	0.1	0.7	0.2	0.1	0.0	100.2	100.6	0.4	n/a
EC	27.4	65.5	0.0	9.2	0.0	0.1	0.0	102.2			$M_{70}C_{30}$

[a] Coefficient of variation.
[b] Typical austenite dendrite composition.
[c] Typical eutectic carbide (EC) composition.

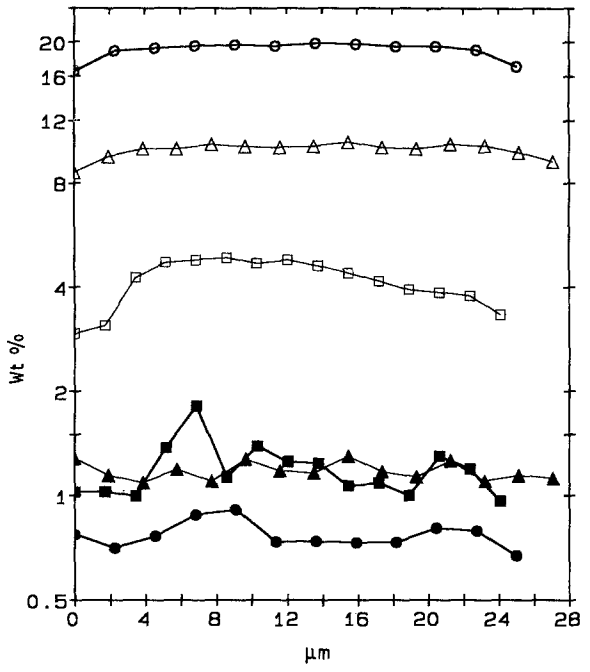

Figure 1 (□, △, ○) Chromium and (■, ▲, ●) carbon analyses across dendrites of Alloys (□, ■) A1, (△, ▲) B1 and (○, ●) C1. Note: ordinate is logarithmic and abscissa is linear.

carbides are formed by the monovariant eutectic reaction of $L \rightarrow M_7C_3 + \gamma$-Fe during metastable solidification.

Microprobe analyses of chromium and carbon for Alloys A1, B1 and C1 are shown in Fig. 1. Inspection of Fig. 1 shows that the carbon content is reasonably uniform across the austenite to the eutectic carbide but the chromium content in all three alloys decreases within $\sim 2\,\mu m$ of the eutectic carbide. The carbon spike shown for Alloy A1 is believed due to an unobserved secondary carbide formed during cooling in the sand mould. Note that Fig. 1 is a semi-log plot. The chromium variation is the opposite of that expected from dendritic microsegregation. The probable explanation is that the austenite adjacent to the eutectic carbide is eutectic austenite and solidified with a lower chromium and carbon content. The uniformity of carbon but not chromium is explained by the faster interstitial diffusion of carbon, which allows a near equilibrium distribution of carbon in the austenite during post-solidification cooling.

From Rivlin's [13] review of the equilibrium ternary Fe–Cr–C system, partial isothermal sections at 1143 K ($\sim$1073 K for Alloy A) and 1273 K (for Alloys B and C) are reproduced in Fig. 2a and b, respectively. Plotted on these isotherms are the microprobe analyses (chromium and carbon) of the γ-Fe matrix for Alloys A1, B1 and C1 taken from Table III. Using these isotherms and the results from microprobe analysis, it is possible to predict the resulting secondary carbides formed during isothermal soaking. For Alloy A, Fig. 2a indicates that the composition is near the boundary of γ-Fe + M_3C. Although Alloy A is not a ternary Fe–Cr–C alloy, this hypothesis is reasonable because nickel is marginally soluble in M_3C, M_7C_3 and $M_{23}C_6$ carbides [15] and by segregating in the austenite expands the γ-Fe + carbide phase field [12].

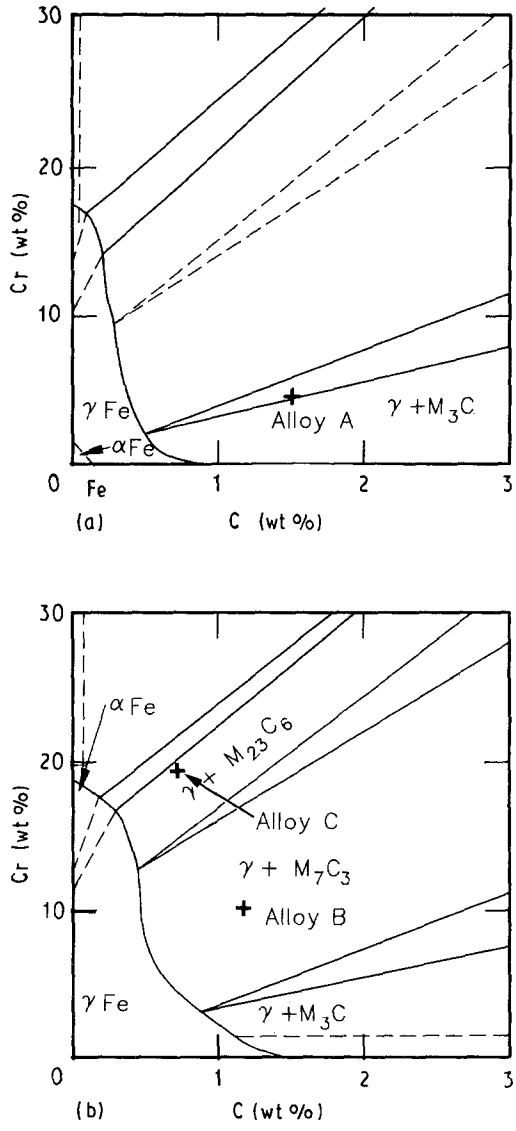

Figure 2 Partial isotherms of the Fe–Cr–C system at (a) 1143 K and (b) 1273 K, after Rivlin [13].

Note that inspection of Fig. 2a shows that the composition of the austenite dendrite in Alloy A is just outside the $\gamma + M_3C$ field. This may be due either to the fact that the isothermal section is that for 1143 K rather than the soak temperature of 1073 K or, more probably, the effect of 7.3 wt % Ni on the boundaries of the $\gamma + M_3C$ field. For Alloys B and C, Fig. 2b shows that the equilibrium state is γ-Fe + M_7C_3 and γ-Fe + $M_{23}C_6$, respectively. The minor concentrations of silicon, manganese and molybdenum for Alloys B and C would be expected to have a negligible effect upon the boundaries of the isothermal section at 1273 K.

To confirm these results partially, microprobe analyses were performed on exposed secondary carbides within Alloys A4 and B4. The procedure involved removing the austenite via deep etching and then traversing the microprobe beam across isolated exposed secondary carbides. An analysis was deemed "accurate" when the weight per cent totals approached 100 ± 2. High or low totals indicate spurious fluorescence conditions, i.e. at the edge of a carbide. The results of these analyses are given in Table IV and are entirely consistent with the above reasoning. It

TABLE IV Microprobe analysis of secondary carbides (wt %)

Alloy	Fe	Cr	Ni	C	Si	Mn	Mo	Total	Stoichiometry
A4	74.3	16.0	1.3	6.6	0.0	1.3	0.0	99.5	$M_{3.04}C$
B4	52.5	35.0	0.2	7.8	0.0	0.8	1.5	98.0	$M_{7.16}C_{2.84}$

should be noted that Basak *et al.* [19] obtained the same results for $M_{7.16}C_{2.84}$ after chemically analysing extracted carbides. The fine secondary carbides in Alloy C4 were beyond the beam resolution and hence could not be analysed.

In the case of Alloy C, transmission electron microscopy work by Pearce and Elwell [20] on a similarly heat treated ~ 28% Cr white cast iron has shown that the secondary carbides are of the $M_{23}C_6$ type.

3.2. Nucleation and growth

After 4 h isothermal heat treatment, Alloys A4, B4 and C4 show superficially similar matrix microstructures of martensite, austenite and secondary carbides when viewed by optical microscopy (Fig. 3a–c. In these photomicrographs, the etchant has darkened the acicular martensite. The secondary carbides (black arrows) and retained austenite were unattacked by the etchant and appear light coloured or white within the dendrites shown in Fig. 3a–c. Furthermore, in Alloy A4, Fig. 3a shows the secondary carbides as having an acicular morphology compared with the more oblate or short rod-like morphologies shown for Alloys B4 and C4 in Fig. 3b and c, respectively.

3.2.1. Alloy A

The composition of Alloy A is similar to that of irons known commercially as NiHard IV [21]. The sequence of nucleation and growth for precipitation of M_3C secondary carbides is shown in Fig. 4a–d.

As clearly shown in all photomicrographs, the M_3C secondary carbides exhibit a plate-like morphology. In the as-cast condition, Fig. 4a, very few M_3C plates have formed upon the slow cooling in the sand mould ($\sim 0.15\ K\ s^{-1}$). Furthermore, it appears that these plates have not nucleated on the M_7C_3 eutectic carbide but within the austenite dendrite. It should be noted that earlier work on Alloy A1 by one of the authors [22] has shown that these eutectic carbides are entirely of the M_7C_3 type and do not possess shells of M_3C.

After 0.25 h at 1073 K, Fig. 4b shows a dramatic increase in the number of M_3C plates. The juxtaposition of these plates appears similar to that of a Widmanstatten mode of growth along preferred crystallographic planes in the austenite dendrite. A study of a possible orientation relationship between the M_3C plates and adjacent austenite has not been carried out but the M_3C plates have sympathetically nucleated on pre-existing M_3C plates [23].

As the isothermal soaking time increases to 0.75 h at 1073 K, Fig. 4c shows that the morphology remains essentially unchanged. Although the number of M_3C plates has further increased, the same general structure is apparent. Similarly to Fig. 4b, the M_3C plates

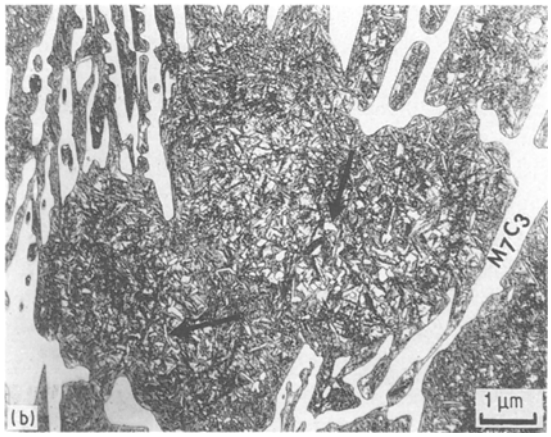

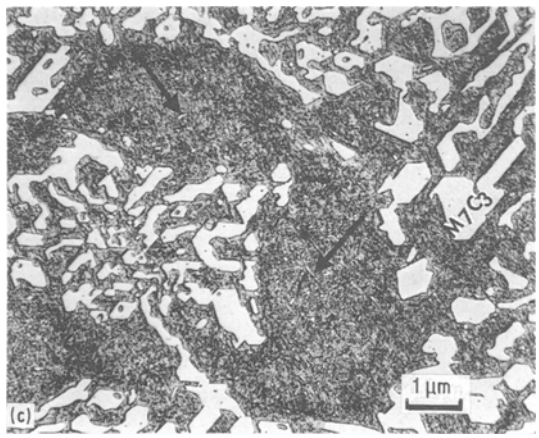

Figure 3 Optical microstructure of irons after heat treating, note numerous secondary carbides in dominantly martensitic dendrites. Etchant: Kallings's Reagent for (a) Alloy A4, and Vilella's Reagent for (b) Alloy B4 and (c) Alloy C4.

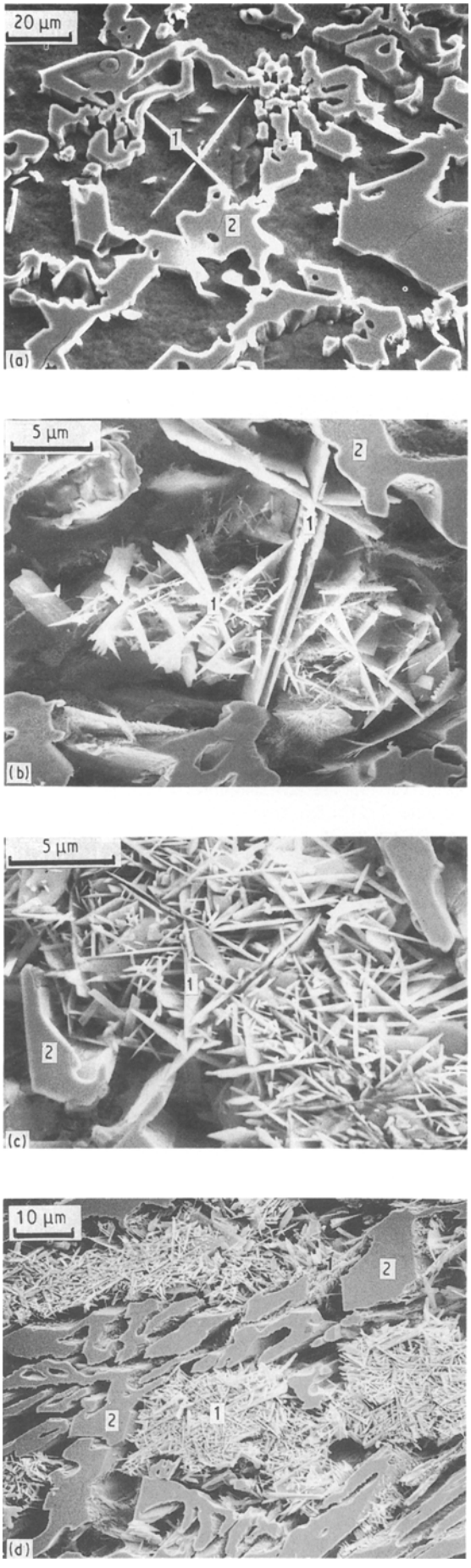

Figure 4 Scanning electron micrographs of Alloy A after deep etching. Note plate-like morphology of M_3C secondary carbides (marked 1) and eutectic morphology of M_7C_3 carbides (2). (a) As-cast, (b) held for 0.25 h at 1073 K, (c) held for 0.75 h at 1073 K, and (d) held for 4 h at 1073 K.

do not appear to nucleate on the M_7C_3 eutectic carbides, with the highest density of M_3C carbides nearer the centre of the austenite dendrite than at the interface between the M_7C_3 and austenite dendrite. Lastly, Fig. 4d shows Alloy A after 4 h at 1073 K. Previously, this same iron was shown optically in Fig. 3a with the matrix described as dominantly martensite. As shown in Fig. 4d, it is apparent that during the soak, a significant proportion of plate-like M_3C carbide precipitated from the austenite which substantially transformed to martensite on cooling. This latter result partly explains the lowered static and dynamic fracture toughness (K_{IC} and K_{ID}) of these irons in the heat-treated condition [7], i.e. the brittle, plate-like M_3C carbides provide numerous crack initiation and growth avenues for intra-dendritic fracture.

3.2.2. Alloy B

In the as-cast condition Alloy B showed virtually no M_7C_3 secondary carbides. This result is in contrast to the observation of several M_3C secondary carbides in Alloy A1. After 0.25 h at 1273 K, Fig. 5a shows the M_7C_3 secondary carbides as having three distinct morphologies. In some locations shown in Fig. 5a the

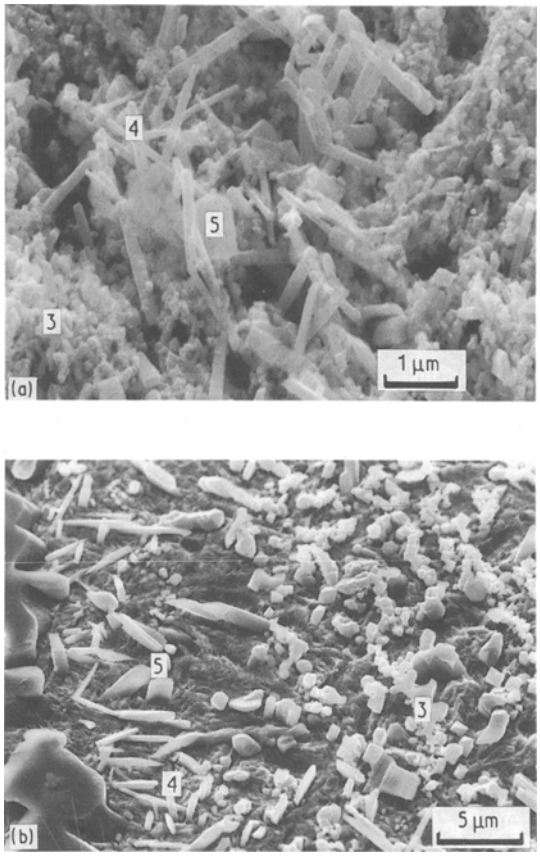

Figure 5 Scanning electron micrographs of Alloys (a) B2 (0.25 h at 1273 K) and (b) B4 (4 h at 1273 K) after deep etching. The M_7C_3 secondary carbides are an aggregate of rod-like particles that appear joined together (3) discrete rods (4), and occasionally as plate-like shapes (5). In (b) (4 h at 1473 K), the carbides are coarser by a factor of approximately 4. Note that there is still no nucleation of M_7C_3 secondary carbide on the eutectic M_7C_3 carbide on the left-hand side of the photograph.

M_7C_3 carbides appear (i) as agglomerates, (ii) as discrete rods, and (iii) as plate-like shapes. By analogy to the growth of eutectic M_7C_3 carbides, the morphologies of the secondary carbides can be inferred. The crystal structure of M_7C_3 is hexagonal [13] and grows as rods of hexagonal cross-section at fast solidification rates [2]. At solidification rates typical of those used in this study, the eutectic M_7C_3 carbide morphology is one of rods and plate-like shapes. Furthermore, transmission electron microscopy work by Pearce [24] has shown that M_7C_3 eutectic rods can cluster together. Hence, the agglomerates and plate-like shapes shown in Fig. 5a are simply extensions of the same basic morphological building block, i.e. the M_7C_3 rod. Inspection of Fig. 5a suggests that extensive nucleation of M_7C_3 carbide occurred in Alloy B during the first 0.25 h soak at 1273 K. Virtually no M_7C_3 secondary carbides were present in the as-cast condition. This suggests that the cooling rate did not allow time for M_7C_3 to nucleate heterogeneously from the austenite during cooling at 0.15 K s^{-1} in the sand mould.

After holding for 4 h at 1273 K, Fig. 5b shows that the principal morphological features remain intact although the carbides are coarser by a factor of approximately 4. The random orientation of the secondary M_7C_3 carbides in Fig. 5b suggests that there is no preferred crystallographic growth relationship with the austenitic matrix.

Similar to Alloy A4, the long isothermal soak experienced by Alloy B4 has resulted in a structure that is primarily composed of elongated M_7C_3 secondary carbides in a substantially martensitic matrix. The presence of these numerous secondary carbides has been noted to decrease the fracture toughness of these irons [7]. Fig. 5b also shows that no M_7C_3 secondary carbide has grown from the M_7C_3 eutectic carbide (left-hand side of photomicrograph) after 4 h. This is in agreement with the results of Pearce [24].

3.2.3. Alloy C

As with Alloy B, there are virtually no secondary carbides in the as-cast condition. Fig. 6a shows Alloy C2 after 0.25 h at 1273 K; the secondary $M_{23}C_6$ carbides have nucleated and grown as very fine fibres which appear to be interconnected. As with Alloy B, there was apparently insufficient time for $M_{23}C_6$ secondary carbides to be nucleated during cooling at 0.3 K s^{-1} in the sand mould.

After holding for 4 h, Fig. 6b shows that there is an infilling of the fibrous network with a slight increase in the thickness of the fibres. Additionally, there is no evidence of the $M_{23}C_6$ secondary carbides nucleating on the eutectic carbides. Pearce and Elwell [20] report that, during heat treatment, a shell of $M_{23}C_6$ forms around the M_7C_3 eutectic carbides. The growth of these $M_{23}C_6$ secondary carbides appears random provided the fine carbide fibres have not moved during preparation of the deep etched specimens.

A similar statement about fracture toughness can be made about Alloy C4. The matrix in this alloy must be also considered to be dominantly composed of elongated $M_{23}C_6$ carbides in a martensitic matrix.

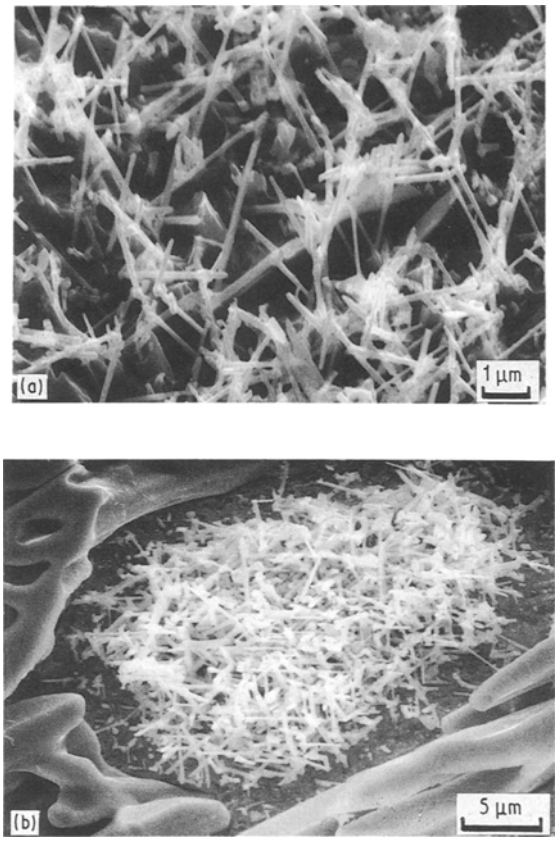

Figure 6 Scanning electron micrographs of alloys (a) C2 (0.25 h at 1273 K) and (b) C4 (4 h at 1273 K) after deep etching. The $M_{23}C_6$ secondary carbides are very fine fibres which appear to be connected. After 4 h, the density of the fibrous network has increased. Note in (b) that the $M_{23}C_6$ secondary carbides have not nucleated on eutectic carbides.

4. Conclusions

1. Compositional information from electron microprobe analyses of austenite dendrites in as-cast Alloys A, B and C, in concert with the appropriate section of the equilibrium Fe–Cr–C phase diagram, predicted the secondary carbides to be M_3C, M_7C_3 and $M_{23}C_6$, respectively.

2. Electron probe analyses of exposed carbides in deep-etched samples confirmed that the secondary carbides in Alloys A and B were M_3C and M_7C_3, respectively.

3. In all alloys, growth of secondary carbides did not occur from eutectic carbides.

4. Consequently, nucleation must occur heterogeneously within the austenite.

5. Growth of these secondary carbides produced different morphologies, namely, the M_3C secondary carbides were plate-like, the M_7C_3 were single rods or rods joined together while the $M_{23}C_6$ were fibrous.

6. M_3C secondary carbides can nucleate and grow in a low-chromium iron, i.e. Alloy A in the as-cast condition (0.15 K s^{-1} cooling rate).

7. M_7C_3 and $M_{23}C_6$ secondary carbides were not observed in high-chromium irons, i.e. Alloys B and C in the as-cast condition (0.15–0.30 K s^{-1} cooling rate).

8. Lastly, after 4 h isothermal soaking, the prior austenite dendrites within all alloys were dominantly composed of secondary carbides within a substantially

martensitic matrix. Therefore, the presence of these carbides should be considered a significant factor in assessing the mechanical and tribological properties of any heat-treated chromium white cast iron.

Acknowledgements

The authors thank Mr John McCracken, CSIRO, for optical metallography, and Mr Keith Collins, US Bureau of Mines, for portions of the scanning electron microscopy investigation.

References

1. ROY ELLIOTT, "Eutectic Solidification Processing" (Butterworths, London, 1983) p. 227.
2. G. L. F. POWELL, *Metals Forum* **3** (1980) 37.
3. R. W. DURMAN and D. W. J. ELWELL, *Br. Foundryman* **78** (1985) 371.
4. G. LAIRD II, R. NEILSEN and N. H. MACMILLAN, *Met. Trans.* **22A** (1991) 1709.
5. J. DODD, *SME Trans.* **270** (1981) 1923.
6. G. J. COX, *Brit. Foundryman* **76** (1983) 129.
7. D. E. DIESBURG and F. BORIK, in "Symposium Materials for the Mining Industry", edited by R. Q. Barr (Climax Molybdenum, Vail, 1974) p. 15.
8. G. LAIRD II, *Trans. AFS* **96** (1988) 799.
9. F. MARATRAY and R. USSEGLIO-NANOT, in "Transformation Characteristics of Chromium and Chromium–Molybdenum White Irons" (Climax Molybdenum, Paris, 1970) p. 7.
10. P. J. PROVIAS, *Canad. Mining Metall. Bull.* **58** (1965) 923.
11. J. T. H. PEARCE, *Trans. AFS* **92** (1984) 599.
12. K. BUNGARDT, E. KUNZE and E. HORN, *Arch. Eisenhurtenw.* **39** (1968) 863.
13. V. G. RIVLIN, *Int. Met. Rev.* **29** (1984) 299.
14. R. S. JACKSON, *J. Iron Steel Inst.* **208** (1970) 163.
15. MATS WALDMENSTROM, *Met. Trans.* **8A** (1977) 1963.
16. L. R. WOODYATT and G. KRAUSS, *ibid.* **7A** (1977) 983.
17. R. BENZ, J. F. ELLIOTT and J. CHIPMAN, *ibid.* **5** (1974) 2235.
18. W. R. THORPE and B. CHICCO, *ibid.* **16A** (1985) 1541.
19. A. BASAK, J. PENNING and J. DILEWIJNS, *Mater. Sci. Technol.* **4** (1988) 22.
20. J. T. H. PEARCE and D. W. L. ELWELL, *J. Mater. Sci. Lett.* **5** (1986) 1063.
21. "Engineering Properties and Applications of Ni-Hard", Report A-70A (Nickel Development Institute, Toronto, Canada).
22. G. LAIRD II, R. R. BROWN and R. E. NIELSON, *Mater. Sci. Tech.* **7** (1991) 631.
23. H. I. AARONSON and C. WELLS, *J. Metals* **8** (1956) 1216.
24. J. T. H. PEARCE, *J. Mater. Sci. Lett.* **2** (1983) 428.

Received 18 October 1990
and accepted 25 March 1991